Physica B 407 (2012) 403–407

Contents lists available at SciVerse ScienceDirect

Physica B

journal homepage: www.elsevier.com/locate/physb

Structure, microstructure and ionic conductivity of the solid solution $LiTi_{2-x}Sn_x(PO_4)_3$

Nedjemeddine Bounar [a,*], Abderrahim Benabbas [a], Farida Bouremmad [a], Patrick Ropa [b], Jean-Claude Carru [b]

[a] LIME Laboratory, University of Jijel, BP 98 Ouled Aissa, 18000, Algeria
[b] LEMCEL Laboratory, BP 717, Calais, 62228, France

ARTICLE INFO

Article history:
Received 18 September 2011
Received in revised form
3 November 2011
Accepted 3 November 2011
Available online 12 November 2011

Keywords:
Impedance spectroscopy
X-ray diffraction
Crystal structure
Ionic conductivity
Microstructure

ABSTRACT

The Nasicon compounds with the composition $LiTi_{2-x}Sn_x(PO_4)_3$ ($x=0$–1.8) were synthesised by the solid state reaction. Their structures were determined from X-ray powder diffraction using Rietveld analysis. All the compositions present the space group R-3c. The refinements show that the Ti and Sn cations are statistically distributed over the same position while the Li ones are exclusively located on the M1 site. The lattice constants *a* and *c* exhibit linear variation over the whole composition range. The bond lengths are in accordance with those of other Nasicon structures. The SEM micrographs of the samples show relative porous microstructures. The ionic conductivity is about 10^{-4}–10^{-5} S cm^{-1}; for the activation energy, a typical value of 0.32 eV is obtained for $x=0.6$ composition whereas significant deviation from linearity in the temperature dependence of the dc conductivity, is observed for the Sn-rich ones. This tendency is discussed along with the structural features.

1. Introduction

Nasicon compounds $A_xB_2(PO_4)_3$ have been extensively investigated owing to their interesting physical properties with potential applications as fast ion conductors [1–9] and low thermal expansions' ceramics [10–12]. The Nasicon structure [13] is built up of corner-sharing BO_6 octahedra and PO_4 tetrahedra leading to a framework of $B_2P_3O_{12}$ formulas with interconnected channels where cations can be inserted in two types of sites usually noted M_1 at 6b (0,0,0) and M_2 at 18e (x,0,1/4) wickoff positions. The great flexibility of this structure allows large chemical substitutions [14–17] and makes it possible that the sites M_1 and M_2 may be empty as in $Nb_2(PO_4)_3$ [18], partially occupied as in [19–21] or completely full as in $Na_4Zr_2(SiO_4)_3$ [22]. The ionic transport in these compounds is due to the migration of the cations through the cavities in the interconnected channels where an order–disorder phenomenon is possible in the partially filled cases. On the other hand, the thermal behaviour is related to the variation of lattice parameters versus temperature generally variable in opposite senses. Thus, the detailed structural characterisation particularly of the atomic positions and the bond lengths is essential to understand the underlying mechanisms and to optimise such properties. The study of the solid solutions $NaTi_2(PO_4)_3$–$NaSn_2(PO_4)_3$ was achieved by Carrasco et al. [23], where an anomalous evolution of lattice parameters either with chemical composition or temperature was encountered.

In this paper, we report the structural characterisation of the phases in the solid solution $LiTi_{2-x}Sn_x(PO_4)_3$ ($x=0$–1.8) using the powder X-ray diffraction and the Rietveld refinements. Their microstructures are studied using scanning electronic microscopy and their ionic conductivity is measured by impedance spectroscopy up to 423 K. The associated activation energy is correlated with the structural parameters.

2. Experimental

Syntheses of $LiTi_{2-x}Sn_x(PO_4)_3$ ($x=0$, 0.2, …, 1.8) were carried out using the conventional solid state reaction techniques. First, stoichiometric mixtures of Li_2CO_3, $(NH_4)_2HPO_4$, TiO_2 and SnO_2 were heated at 673 K for 5 h in order to decompose the ammonium phosphate and lithium carbonate. In a second step, the finely ground samples were heated twice at 1473 K for 48 h at each time. The X-ray diffraction patterns were recorded at room temperature with a D8-Advance Diffractometer of Bruker AXS (CuKα radiation) equipped with a curved graphite monochromator in the secondary beam. The data were collected in the 14°–104°(2θ) range in steps of 0.02° and a counting time of 16 s per step. The refinement of the structure by the Rietveld method was performed using the Rietica program [24]. The surface morphologies of the pellets were observed with scanning

* Corresponding author. Fax: +213 34501189.
E-mail address: bounar_nedjemeddine@univ-jijel.dz (N. Bounar).

0921-4526/$ - see front matter © 2011 Elsevier B.V. All rights reserved.
doi:10.1016/j.physb.2011.11.006

electron microscopy on a PHILIPS XL 30 apparatus. For the impedance spectroscopy measurements, powders were ground and pelletized under a pressure of 10 t. Then, the pellets were sintered at 1473 K for 24 h. Impedance measurements were done from room temperature up to 423 K; a Hewlett Packard 4284 A apparatus was used, in a frequency range from 20 Hz to 1 MHz and with an oscillating voltage of 100 mV.

3. Results and discussion

Preliminary unit-cell parameters determination was obtained by full pattern decomposition according to the Lebail method. Starting structural parameters for Rietveld refinement were taken from the usual Nasicon data in the R-3c space group. The structural refinements were carried out with a polynomial function for the background, pseudo-voigt function for the peak-shape; the other refined parameters include scale factor, lattice parameters, atomic coordinates and isotropic thermal parameters. The titanium and tin cations were assumed to be randomly distributed over the same crystallographic site, with the respective occupancies corresponding to the nominal composition. Details of all the final structural models over the composition range are given in Table 1. For example, the final Rietveld plot for the composition $x=1$ is presented in Fig. 1.

The unit-cell parameters for the compound $LiTi_2(PO4)_3$ ($x=0$) are in good agreement with those reported in previous works [25,26]. In all the compositions, the M1 site is fully occupied whereas M2 one is empty. The space group R-3c is here conserved over the whole composition range, unlike the Na-Analogue solid solution [23]. In this case, this space group is only adopted for $x \leq 1$ and a transition to R-3 is noted for $x > 1$. A related feature is observed concerning the evolution of lattice constants versus x; in $LiTi_{2-x}Sn_x(PO_4)_3$ phases, we note a nearly linear increase for both a and c parameters (Fig. 2). However, an unusual behaviour is encountered for Na-Analogue phases where the a parameter passes through a maximum at $x=1$.

The increase of the inter-atomic distances in the Ti/SnO_6 octahedra (Table 2) can be associated with the increase of the averaged cationic size along with this substitution. The distances P–O (Table 2) are in good agreement with those typically observed in Nasicon phosphates. The Li–O bond lengths (Table 2) have also slightly increased; the same evolution was observed in other Nasicon structures as pointed out particularly by Alami et al. [27]. The details of the Nasicon structures have been discussed by some authors [28–31].

This structure can be described as built up of infinite 1D ribbons $O_3BO_3M_1O_3BO_3$ connected by PO_4 tetrahedra (Fig. 3). The spatial distribution of ionic charges (Fig. 4) on these ribbons gives

Table 1
Crystal data and structure refinement versus x for $LiTi_{2-x}Sn_x(PO_4)_3$.

	$x=0$	$x=0.2$	$x=0.4$	$x=0.6$	$x=0.8$	$x=1.0$	$x=1.2$	$x=1.4$	$x=1.6$	$x=1.8$
a (Å)	8.5147(2)	8.5230(3)	8.53850(7)	8.5491(1)	8.5586(2)	8.5706(1)	8.58670(9)	8.59830(9)	8.6121(2)	8.62180(9)
c (Å)	20.8782(6)	20.9340(9)	21.0150(4)	21.0473(7)	21.1000(8)	21.1742(5)	21.2280(4)	21.2868(4)	21.3574(6)	21.4015(4)
z (Ti/Sn)	0.1471(1)	0.1465(6)	0.1460(5)	0.1457(5)	0.1450(2)	0.1448(4)	0.1441(3)	0.1435(4)	0.1431(3)	0.1425(4)
x (P)	0.2894(3)	0.2890(3)	0.2892(2)	0.2896(2)	0.2902(4)	0.2908(2)	0.2903(2)	0.2907(3)	0.2915(3)	0.2908(3)
x (O1)	0.1907(5)	0.1912(5)	0.1914(3)	0.1909(4)	0.1905(4)	0.1913(1)	0.1915(4)	0.1921(6)	0.1918(5)	0.1922(5)
y (O1)	−0.0015(5)	−0.0018(5)	−0.0024(4)	−0.0031(5)	−0.0042(5)	−0.0047(4)	−0.0053(4)	−0.0061(7)	−0.0065(5)	−0.0073(6)
z (O1)	0.1903(2)	0.1901(2)	0.1899(1)	0.1904(1)	0.1911(1)	0.1897(1)	0.1906(1)	0.1900(2)	0.1908(1)	0.1912(2)
x (O2)	0.1835(4)	0.1838(4)	0.1844(3)	0.1847(4)	0.1853(4)	0.1860(3)	0.1866(3)	0.1872(5)	0.1878(4)	0.1885(4)
y (O2)	0.1636(4)	0.1640(4)	0.1644(3)	0.1648(3)	0.1655(3)	0.1652(3)	0.1662(3)	0.1671(5)	0.1669(4)	0.1675(5)
z (O2)	0.0813(2)	0.0816(2)	0.0814(1)	0.0810(1)	0.0808(1)	0.0814(2)	0.0821(1)	0.0813(2)	0.0819(2)	0.0815(2)
Rp (%)	9.24	7.22	7.59	9.32	8.52	7.80	8.52	10.01	9.34	10.01
Rwp (%)	11.84	9.25	10.00	11.92	10.67	9.92	10.67	12.64	11.61	12.37

*Wickoff positions: Ti/Sn at **12c** (0, 0, z), P at **18e** (x,0,1/4), O1 and O2 at **36f** (x, y, z).

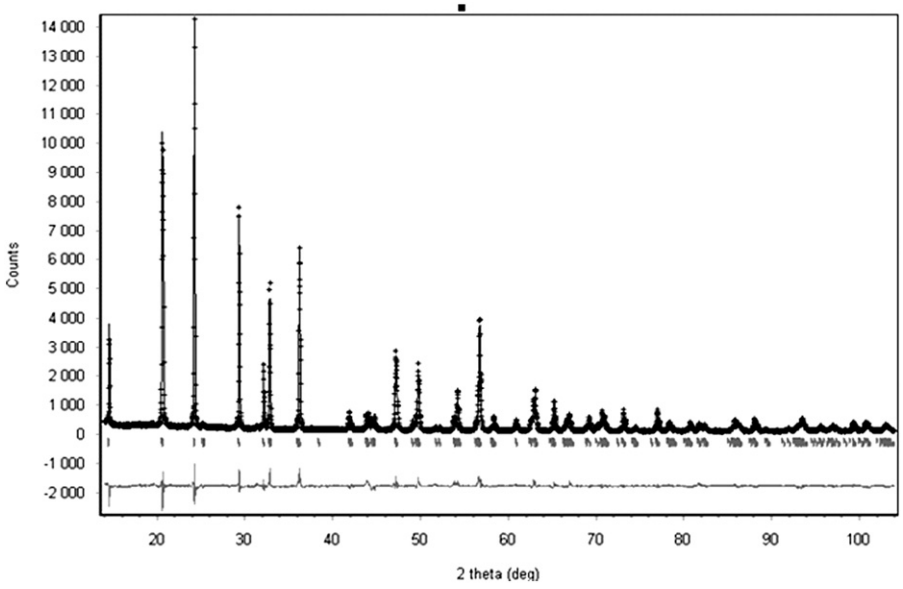

Fig. 1. Rietvelt plot: observed–calculated and difference profile for $LiTiSn(PO_4)_3$ ($x=1$).

particularly rise to the displacement of the B cations along *c* towards O1 anions. As consequence, it is the presence of these opposite stresses on adjacent BO6 octahedra, which induces the split of the O1 anions in the (a, b) plane and the increasing of the corresponding lattice parameters. The off-centring of the B cations in their octahedra and its magnitude as indicated by the difference between the bond lengths B–O1 and B–O2 and also the distances O1–O1 (Table 3) confirm this view point. In this context, one can note that for the same type of A (or B) cation, the smaller the cation B (or A) i.e. with more dense positive charge, the larger is this effect.

The distance O1–O1 has a direct influence on the value of the a parameter, which explains the shortening of this parameter with the increase of the A cation size in the M1 site. This situation is achieved by the chemical nature of this cation or with rising temperature. Furthermore, the slope of this shrinking should be more reduced for larger B cations [37]. It is obvious that if the M1 site is empty, the distance O2–O2 along *c* will be enhanced and the off-centring of the B cations will be reversed, as shown for example in $Nb_2(PO_4)_3$ [18] and $NbTi(PO_4)_3$ [38] where the corresponding bond lengths (B–O1, B–O2) are of (1.993 Å, 1.968 Å) and (1.978 Å, 1.924 Å), respectively. Finally, each kind of cation, A or B, will influence the averaged size of the coordination polyhedron around the other one. In fact, the electron density of the oxygen anions coordinating larger cation in one site will occupy more of volume and consequently will be more reduced, which in return will lengthen their distances with the other cation. As the case of Li cation mentioned above [27], the Na–O bond lengths in the Nasicon compounds are also found to increase with the B cation size, as shown by the structures of $NaTi_2(PO_4)_3$ [32], $NaMo_2(PO_4)_3$ [39] and $NaZr_2(PO_4)_3$ [35] where the distances Na–O are of 2.427 Å, 2.467 Å and 2.550 Å, respectively. Owing to its coordination polyhedron, the M2 site is of 3D character. Depending on its occupancy, the presence of cations in this site can attenuate or overcome the effect of the cations in the M1 one

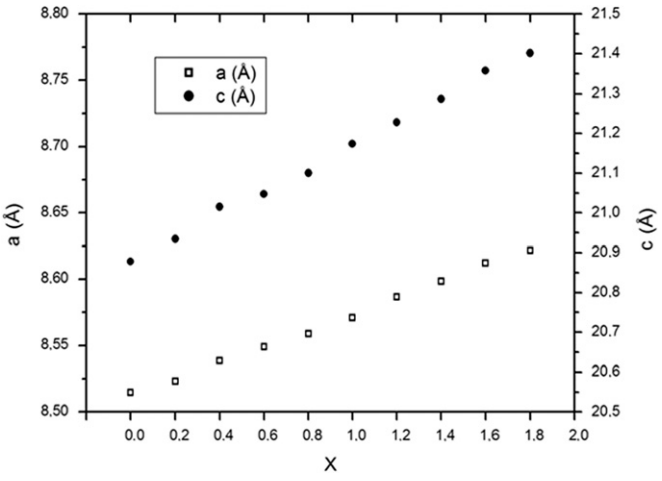

Fig. 2. Evolution of the unit-cell constants versus *x* for $LiTi_{2-x}Sn_x(PO_4)_3$.

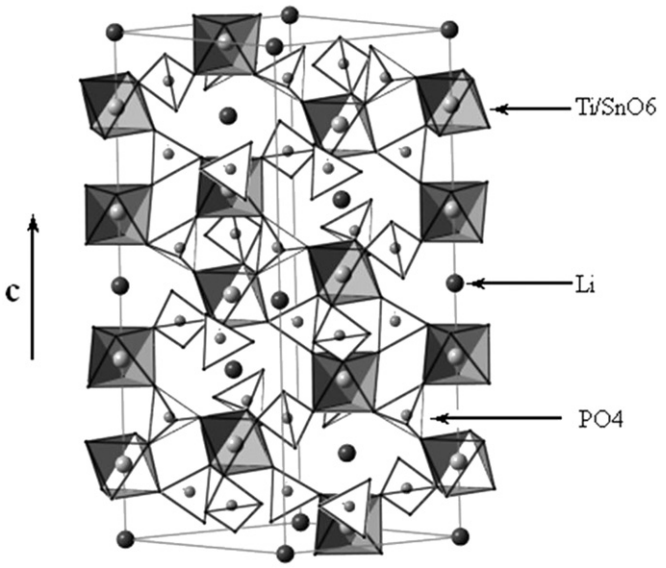

Fig. 3. The Nasicon crystal structure.

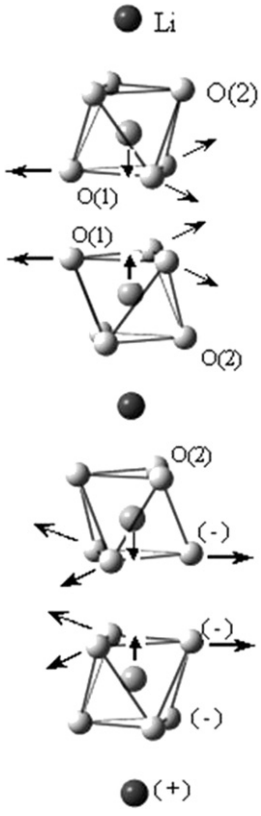

Fig. 4. The opposite local stresses applied on adjacent BO6 octahedra in the $O_3BO_3M_1O_3BO_3$ ribbons.

Table 2
Bonds' lengths versus *x* for $LiTi_{2-x}Sn_x(PO_4)_3$.

d (Å)	$x=0$	$x=0.2$	$x=0.4$	$x=0.6$	$x=0.8$	$x=1.0$	$x=1.2$	$x=1.4$	$x=1.6$	$x=1.8$
Li–O2	2.255(4)	2.266(3)	2.273(2)	2.272(3)	2.276(3)	2.293(2)	2.314(3)	2.310(4)	2.327(2)	2.329(3)
Ti/Sn–O1	1.863(4)	1.875(3)	1.886(2)	1.895(3)	1.914(3)	1.913(2)	1.938(3)	1.949(4)	1.965(2)	1.985(3)
Ti/Sn–O2	2.023(3)	2.016(2)	2.020(2)	2.027(3)	2.027(3)	2.023(2)	2.012(3)	2.024(4)	2.016(2)	2.021(3)
P–O1	1.500(4)	1.502(4)	1.509(2)	1.505(3)	1.498(3)	1.525(3)	1.508(3)	1.519(4)	1.514(2)	1.502(4)
P–O2	1.558(3)	1.559(3)	1.556(2)	1.554(3)	1.547(3)	1.543(2)	1.542(2)	1.536(4)	1.532(2)	1.532(3)

Table 3
Influence of the nature of A and B cations on some structural details of the Nasicon Structures.

Compound	a (Å)	c (Å)	B–O1 (Å)	B–O2 (Å)	O1–O1 (Å)
$NaTi_2(PO_4)_3$ [32]	8.480	21.770	1.895	1.975	2.787
$KTi_2(PO_4)_3$ [33]	8.367	23.074	1.918	1.942	2.720
$RbTi_2(PO_4)_3$ [34]	8.290	23.530	1.927	1.944	2.707
$NaZr_2(PO_4)_3$ [35]	8.815	22.746	2.045	2.068	2.945
$KZr_2(PO_4)_3$ [36]	8.710	23.890	2.060	2.066	2.915

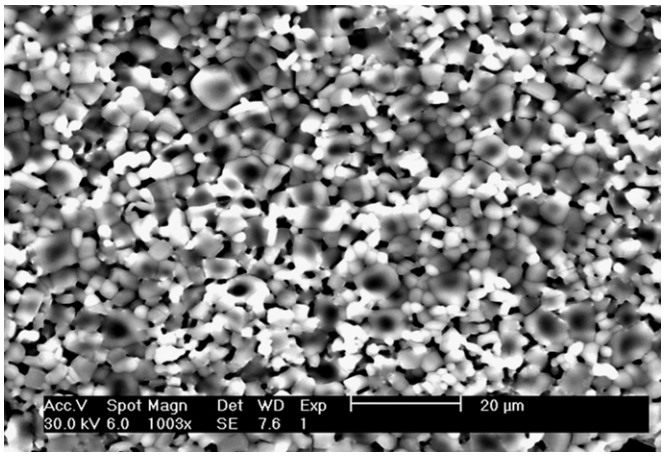

Fig. 5. SEM micrograph of $LiTi_{0.6}Sn_{1.4}(PO_4)_3$ ($x=1.4$).

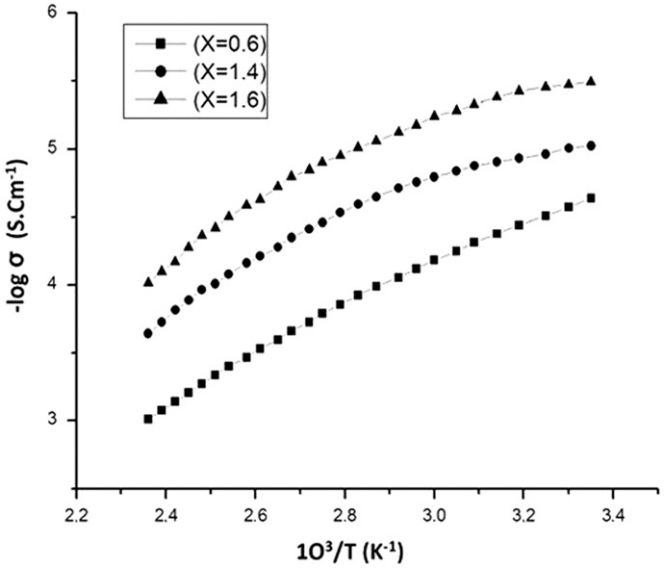

Fig. 6. Temperature dependence of the dc conductivity of the $x=0.6$, 1.4 and 1.6 compositions.

on the variation of the *a* parameter. Concerning the *c* axis, the two kinds of sites M1 and M2 have cumulative and positive expansive effects. Fig. 5 shows an example of the SEM micrographs of our samples. The presence of porosity is usual in such materials [40] and their densification requires hot pressure sintering.

Impedance spectroscopy measurements were achieved from room temperature up to 423 K, for three compositions corresponding to $x=0.6$, 1.4 and 1.6. The bulk resistance is determined by extrapolating the left intercept of the impedance curve with the real axis in the Nyquist representation and the ionic conductivity σ is deduced from the relation $\sigma=L/(RS)$, where L is the thickness and S the area of the pellet. For examples the values of σ at 373 K are of (2.17×10^{-4}), (4.46×10^{-5}) and (1.59×10^{-5}) S cm^{-1} for $LiTi_{1.4}Sn_{0.6}(PO_4)_3$, $LiTi_{0.6}Sn_{1.4}(PO_4)_3$ and $LiTi_{0.4}Sn_{1.6}(PO_4)_3$, respectively. These results are in agreement with previous works [41,42]; σ seems decreasing with the increase of the averaged size of the B cations, which proves that the underlying mechanism is not related exclusively to steric effects and the energetic profile through the conduction path should be considered.

The activation energy E_a associated with the ionic motion, according to the Arrhenius law can be evaluated from the variation of dc conductivity ($\log\sigma$) versus inverse temperature (Fig. 6). Linear curve is encountered for the $x=0.6$ composition with an activation energy of 0.32 eV; for the Sn-rich compositions, one can observe significant deviation from linearity, which can be related to a variable range hopping mechanism [43] or to a partial ordering of the Ti and Sn cations not detected by the X-ray structural analysis. Moreover, the linear behaviour requires that E_a has to be constant over the temperature range; this fact is practically verified along with smooth variation of structural features. However, the large thermal expansion of the *c* parameter [37] in the Nasicon structure can also induce a variation of the activation energy and causes the curvature of $\log\sigma$ versus $1/T$.

4. Conclusion

The structural study of the solid solution $LiTi_{2-x}Sn_x(PO_4)_3$ shows linear variations of the unit-cell parameters, the conservation of the space group R-3c over the whole composition range and the location of the Li cations on the M1 sites as confirmed by the off-centring of the Ti/Sn cations in their octahedra. The macrostructures are relatively porous. The ionic conductivity is of the order of 10^{-4}–10^{-5} S cm^{-1}. The variation of activation energy with the temperature is related to the crystal structure evolution.

References

[1] H.Y.-P. Hong, Mater. Res. Bull. 11 (1976) 173.
[2] J.B. Goodenough, H.Y.-P. Hong, J.A. Kafalas, Mater. Res. Bull. 11 (1976) 203.
[3] F. D'Yvoire, M. Pintard-Screpel, E. Bretey, M. de Larochere, Solid State Ionics 9–10 (1983) 851.
[4] T. Maruyama, S. Sasaki, Y. Saito, Solid State Ionics 23 (1987) 107.
[5] C. Delmas, A. Nadiri, J.L. Soubeyroux, Solid State Ionics 28–30 (1988) 419.
[6] C.J. Leo, B.V.R. Chowdari, G.V. Subba Rao, J.L. Souquet, Mater. Res. Bull. 37 (2002) 1419.
[7] F. Brunet, N. Bagdassarov, R. iletich, Solid State Ionics 159 (2003) 35.
[8] C.J. Leo, G.V. SubbaRao, B.V.R. Chowdari, Solid State Ionics 159 (2003) 357.
[9] X.H. Liu, T. Saito, T. Doi, S. Okada, J.-I. Yamaki, J. Power Sources 189 (2009) 706.
[10] R. Roy, D.K. Agrawal, J. Alamo, R.A. Roy, Mater. Res. Bull. 19 (1984) 471.
[11] N. Chakraborty, D. Basu, W. Fischer, J. Eur. Ceram. Soc. 25 (2005) 1885.
[12] N. Anantharamulu, K.K. Rao, M. Vithal, G. Prasad, J. Alloys Compd. 479 (2009) 684.
[13] L. Hagman, P. Kierkegaard, Acta Chem. Scand. 22 (1968) 1822.
[14] O. Nakamura, Y. Saito, M. Kodama, Y. Yamamoto, Solid State Ionics 89 (1996) 159.
[15] A. El Jazouli, A. El Bouari, H. Fakrane, A. Housni, M. Lamire, I. Mansouri, R. Olazcuaga, G. Le Flem, J. Alloys Compd. 262–263 (1997) 49.
[16] S.R.S. Prabaharan, A. Fauzi, M.S. Michael, K.M. Begam, Solid State Ionics 171 (2004) 157.
[17] Y. Kim, J.B. Goodenough, Electrochem. Commun. 10 (2008) 497.
[18] A. Leclaire, M.-M. Borel, A. Grandin, B. Raveau, Acta Crystallogr. C45 (1989) 699.
[19] J.P. Boilot, G. Collin, Ph. Colomban, Mater. Res. Bull. 22 (1987) 669.
[20] C. Veríssimo, F.M.S. Garrido, O.L. Alves, P. Calle, A. Martínez-Juárez, J.E. Iglesias, J.M. Rojo, Solid State Ionics 100 (1997) 127.
[21] M. Barré, M.P. Crosnier-Lopez, F. Le Berre, E. Suard, J.L. Fourquet, J. Solid State Chem. 180 (2007) 1011.
[22] D.T. Qui, J.J. Capponi, J.C. Joubert, R.D. Shannon, J. Solid State Chem. 39 (1981) 219.
[23] M.P. Carrasco, M.C. Guillem, J. Alamo, Mater. Res. Bull. 27 (1992) 603.
[24] C.J. Howard, B.A. Hunter, D.A.J. Swinkels, Rietica IUCR Powder Diffr. 22 (1997) 21.
[25] G.X. Wang, D.H. Bradhurst, S.X. Dou, H.K. Liu, J. Power Sources 124 (2003) 231.
[26] R. Masse, Bull. Soc. Fr. Min. Crist. 93 (1970) 500.

[27] M. Alami, R. Brochu, J.L. Soubeyroux, P. Gravereau, G. Le Flem, P. Hagenmuller, J. Solid State Chem. 90 (1991) 185.
[28] C. Delmas, J.C. Viala, R. Olazcuaga, G. Le Flem, P. Hagenmuller, F. Cherkaoui, R. Brochu, Mater. Res. Bull. 16 (1981) 83.
[29] J. Alamo, Solid State Ionics 63–65 (1993) 547.
[30] A. Aatiq, C. Delmas, A. El Jazouli, J. Solid State Chem. 158 (2001) 169.
[31] A. Aatiq, M. Ménétrier, A. El Jazouli, C. Delmas, Solid State Ionics 150 (2002) 391.
[32] R. Shimanouchi-Futagami, H. Nishizawa, Kin.Daigaku Rik. Kenk. Hokoku 16 (1995) 13.
[33] E.S. Lunezheva, B.A. Maksimov, O.K. Mel'nikov, Kristallogr. 34 (1989) 1119.
[34] R. Duhlev, Acta Crystallogr. C50 (1994) 1525.
[35] H. Hong, Mater. Res. Bull. 11 (1976) 173.
[36] M. Sljukic, B. Matkovic, B. Prodic, D. Anderson, Zeits. fur Kristallogr 130 (1969) 148.
[37] M.P. Carrasco, M.C. Guillem, J. Alamo, Mater. Res. Bull. 28 (1993) 547.
[38] F.J. Berry, C. Greaves, J.F. Marco, J. Solid State Chem. 96 (1992) 408.
[39] K.H. Lii, J.J. Chen, S.L. Wang, J. Solid State Chem. 78 (1989) 93.
[40] J. Wolfenstine, J.L. Allen, J. Sumner, J. Sakamoto, Solid State Ionics 180 (2009) 961.
[41] K. Arbi, M. Tabellout, J. Sanz, Solid State Ionics 180 (2010) 1613.
[42] A. Martinez-Juarez, J.M. Amarilla, J.E. Iglesias, J.M. Rojo, J. Braz. Chem. Soc. 8 (1997) 261.
[43] N.F. Mott, E.A. Davis, Electronic Processes in Non-Crystaline Materials, Clarendon Press, Oxford, 1979.